



ELSEVIER

Colloids and Surfaces A: Physicochem. Eng. Aspects 217 (2003) 81–92

COLLOIDS  
AND  
SURFACES

A

www.elsevier.com/locate/colsurfa

# Comparison of colloid investigations by single particle analytical techniques—a case study on thorium-oxyhydroxides

C. Walther\*

*Institut für Nukleare Entsorgung, Forschungszentrum Karlsruhe, Postfach 3640, D76021 Karlsruhe, Germany*

## Abstract

Characterization of complex systems such as colloids calls for the combination of a multitude of analytical methods. This work reviews some of the most common techniques used to gain information on the particle size distribution of a colloidal suspension. Fractionation by filtration or centrifugation is discussed as well as flow field fractionation and electron- and atomic-force microscopy. Since these delicately balanced systems are to be characterized with as little perturbation as possible, this work lays special emphasis on non-invasive methods such as light scattering (photon correlation spectroscopy (PCS), static light scattering; single particle counter) and laser induced breakdown detection, an in-situ method, which opens up a wide operational dynamic range, covering three orders of magnitude in size (5–1000 nm) and seven orders of magnitude in particle concentration (1 ppt–several ppm). Advantages and shortcomings of each technique are illuminated by means of an example, the characterization of  $\text{ThO}_n(\text{OH})_m$ -colloids in over-saturated thorium solutions. Results obtained by atomic force microscopy (AFM)-, scanning electron microscopy (SEM)-, transmission electron microscopy (TEM)-, PCS- and laser induced breakdown detection (LIBD) measurements are compared and discussed.

© 2002 Elsevier Science B.V. All rights reserved.

*Keywords:* Colloid; Aquatic; Thorium; Breakdown; Single particle

## 1. Introduction

Colloids are of common interest to many different research fields, and the methods applied to their characterization likewise are of diverse origins. While their presence is undesired in clean process liquids, e.g. for semiconductor manufacturing [1] or for the primary coolant of nuclear power plants [2–5], they are conveniently used for the design of ‘new materials’ [6,7] and also of

catalysts [8]. In natural aquifers, aquatic colloids appear to play a carrier role for the migration of pollutants, in particular heavy metal ions [9] or radionuclides [10,11], which in addition show a strong tendency to form ‘true’ colloids [12,13].

In the aquifer the size regime spans several orders of magnitude (1 nm–several  $\mu\text{m}$ ) and typical concentrations can vary from  $10^5$  to  $10^{15}$   $\text{l}^{-1}$  water [14]. However, due to their small size the surface to volume or mass ratio is very large (several  $10 \text{ m}^2 \text{ g}^{-1}$ ) and even at moderate concentrations the net surface involved in interactions with the chemical surrounding should not be

\* Tel.: +49-7247-82-6064; fax: +49-7247-82-3927.

E-mail address: walther@ine.fzk.de (C. Walther).

underestimated. In conjunction with very complex chemical properties the combination of many complementary methods is required to achieve a closed picture. Hence, colloid science represents a highly interdisciplinary field of research.

The particle size distribution (PSD) is one very important parameter of a colloidal suspension. Generally, samples show broad size distributions and since one single detection method might not cover this large range with adequate sensitivity and resolving power, several techniques have to be combined. Table 1 lists the techniques applied most frequently. The three classical separation (pre-fractionation) techniques, centrifugation, filtration, and sedimentation which are discussed in detail, e.g. in [15] and references therein, are listed along with sedimentation, which was shown to work for colloids as small as 10 nm [16]. Field flow fractionation (FFF) cannot be operated as ‘stand alone’ technique, but rather is to be considered a pre-fractionation stage followed by a particle detection unit which determines the sensitivity. A very detailed review is given in [17]. Three kinds of microscopy and four detection methods based on particle-light interaction, follow. The data on accessible sizes and concentrations may be understood as rules of thumb only. The detection limit (DL) may strongly depend on particle size (e.g. for

photon correlation spectroscopy, PCS, the DL scales with the 6th power of the diameter). In many cases refined versions of the method exist, allowing the investigation of extended size ranges and the same holds for the particle concentration. The single particle counter (SPC), a method based on static light scattering, for instance, is capable of detecting colloids larger than 50 nm at very low concentrations ( $< 10^4 \text{ ml}^{-1}$ ) [3,4,18]. Also particle composition may influence the detection limit (e.g. contrast in scanning electron microscopy, SEM, is strongly enhanced for heavy elements). For each method it is indicated whether the properties of single particles (S) or the mean values for the population (P) are mapped. S(P) indicates that the properties of the population are gained by detecting single particle events, but one event by itself cannot meaningfully be interpreted. Suitability for in-situ measurements and the extent of sample preparation necessary are itemized. Finally, the methods are categorized according to whether the system is strongly disturbed (invasiveness) and whether the same particle that has been used for size measurement is still available for further investigations (destructiveness).

One of the standard size characterization techniques nowadays is photon correlation spectroscopy (PCS), which allows in situ measurements,

Table 1  
Methods for determination of colloid size and concentration

Method	Size (nm)	Concentration	Statistics	In situ	Preparation	Invasive	Destructive
Centrifugation	50–10 <sup>5</sup>	ppb	P	(x)	Med.	x	(–)
Filtration	> 1	ppb	P	(x)	Med.	x	(–)
Sedimentation	> 10	ppm	P	–	Med.	x	x
Field flow fractionation, FFF	> 2	DM	P	–	Low	x	–
Transmission electron microscopy, TEM	0.5–100	ppm	S	–	High	x	x
Scanning electron microscopy, SEM	> 10	ppm	S	–	High	x	x
Atomic force microscopy, AFM	1–1000	ppm	S	(x)	Med.	(x)	(–)
Static light scattering, SLS	> 100	ppm	S(P)	x	None	–	–
Single particle counter, SPC	> 30	ppq	S(P)	x	None	–	–
Photon correlation spectroscopy, PCS	2–2000	ppm	S(P)	x	None	–	–
Laser induced breakdown detection, LIBD	> 5	ppt	S(P)	x	None	–	x

Given sizes reflect the most common range of operation and the detectable concentrations may vary strongly with colloid size. For FFF the concentration range depends on the sensitivity of detection method (DM). Column ‘Statistics’ indicates whether the properties of S)ingle particles or of the whole P)opulation are determined. S(P) means detection of single particles but statistical relevance only for an average over many measurements. Next, the suitability for in-situ measurements and the preparative work necessary are given. Finally the methods are classified, whether invasive (disturbing the system as a whole) and destructive (is the very particle measured available for additional investigations).

but is restricted to suspensions of large colloids or high number density. Electron microscopy certainly is the most powerful technique for investigating nanosystems, including element-composition and internal structure, but the initial state of aquatic colloids is disturbed during sample preparation. Atom force microscopy (AFM) is a non-destructive method of atomic resolution, but requires a relatively concentrated colloid suspension, which means that a condensation of sample might be necessary for the colloid characterization. Advantages and limitations of these methods are considered in the context of colloid formation in over-saturated solutions, a topic being investigated in the framework of gaining thermodynamic solubility data of actinides.

## 2. The colloids

In continuation of previous work the formation of colloids in over-saturated thorium solutions is studied [19,20]. Acidic solutions containing a well defined concentration of Th(IV) in 0.5 M HCl/NaCl were prepared. By coulometric titration the pH was increased in very small steps until the solubility was just exceeded, initiating the formation of small colloids. Fig. 1 shows the corresponding solubility diagram, where the Th(IV) concentration is plotted versus  $H^+$  concentration on a log-log scale. Two domains have to be distinguished: Titrations in the pH range 1.5–2.5 lead to the formation of small microcrystalline  $ThO_2 \cdot H_2O(s)$  colloids which subsequently agglomerate to a microcrystalline precipitate [20]. At pH 3–5 hydrolysis and poly-nucleation causes the formation of amorphous thorium hydroxide colloids. The  $H^+$  and Th(IV) concentrations at the onset of colloid formation define the solubility of  $Th(OH)_4(am)$ .

Three suspensions are investigated in the following, denominated *A*, *B* and *C* in Fig. 1. *A* refers to the ‘ $ThO_2$  domain’, at a Th(IV) concentration of  $2.5 \times 10^{-3}$  M at pH 1.9. Suspension *B* contains about the same amount of Th(IV) ( $3 \times 10^{-3}$  M) at pH 3.8, hence being in the ‘ $Th(OH)_4$  colloid domain’, at strong oversaturation (vertical distance to the solubility curve) but still showing no

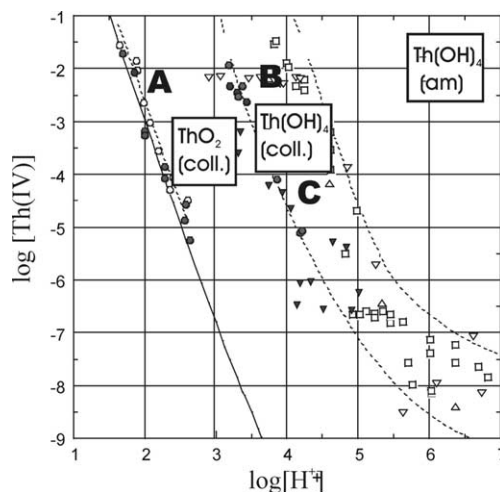


Fig. 1. Solubility diagram of Th(IV). When the solubility is exceeded, colloids are formed: thorium dioxide at pH 1.5–2.5 (lower curve) and thorium hydroxide at pH > 3 (between the two dashed curves). Three samples *A*, *B*, and *C* are further investigated. Experimental data and investigations are taken from [19–21].

observable precipitation. Suspension *C* belongs to the same domain, but at lower concentration ( $[Th(IV)] = 6.3 \times 10^{-5}$  M, pH 4.1) and closer to the solubility curve. Combination pH electrodes (type ROSS, Orion) are used to determine the  $H^+$  concentration in 0.5 M NaCl solution. They are calibrated against standard pH buffers (pH 1–10, Merck) and standard solutions  $x$  M HCl/(0.5– $x$ ) M NaCl with  $x$  in the range 0.001–0.1. This yields the relation between the  $H^+$  concentration and measured  $pH_{exp}$  containing the activity coefficient ‘*A*’ [21].

$$-\log[H^+] = pH_{exp} + A$$

All suspensions were aged for at least six months in order to reach equilibrium.

## 3. The analytical methods

### 3.1. Photon correlation spectroscopy

Since PCS is an easy to use in-situ method [22], allowing non-invasive, non-destructive colloid characterization without sample preparation, we tried to apply this method to our samples. Colloids

between  $\approx 2$  nm and  $2 \mu\text{m}$  can be detected, however the sensitivity strongly depends on the particle size (Fig. 2) and decreases proportionally to the 6th power of the inverse particle diameter below 100 nm [23]. The suspension is available for further investigations, e.g. elemental analysis or can be measured again in order to observe time evolution. Instruments of many different manufacturers are commercially available allowing ‘hands-off’ operation without need for calibration. Single events are detected, but can only be evaluated to statistical relevance in large number and reflect values averaged over the sample. Typically more than  $10^5$  counts are summed up for the correlation function, which takes only minutes by use of intense laser light sources. A model suspension of 10 ppm  $\text{ZrO}_2$ -colloids of 100 nm diameter (Alfa Aesar, Zirconium(IV) oxide, colloidal dispersion) yields a smooth correlation function corresponding to a mean size of 92.7 nm, in good agreement with the specification of the manufacturer (100 nm). In contrast for all three thorium samples investigated here, the correlation function decays too fast due to either very small colloid diameter and/or low concentration (see below). This shows the most severe drawback of this method, the low sensitivity for particles below

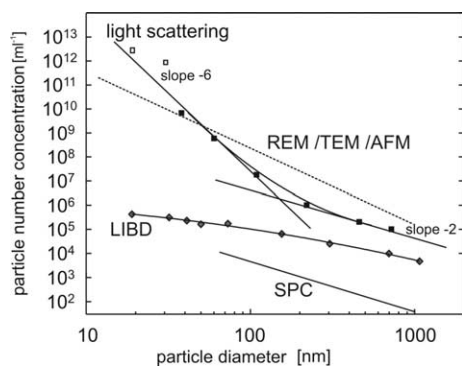


Fig. 2. Sensitivity of selected colloid characterization methods. In general light scattering methods suffer from a strong sensitivity-decrease for particles below 100 nm ( $\lambda/4$ ). However, the SPC based on static light scattering allows to detect colloids  $> 30$  nm at ultratrace levels. LIBD shows a less pronounced size-dependence and is applicable to colloids  $> 5$  nm. The sensitivity of electron- and atomic force microscopy depends strongly on sample preparation and can deviate from the values given by the dotted curve.

100 nm. Furthermore, PCS is limited in resolving multimodal particle distributions. A comparatively small fraction of big particles can cause a large signal masking the presence of a vast surplus of small colloids. A number of sophisticated analysis and data filtering techniques were developed to gain information on size distributions. In all cases, in order to obtain concentration information from the scattered light intensity, a uniform shape of the particles must be assumed and the refractive index of the colloids must be known.

### 3.2. Electron microscopy

Next, the samples were investigated by electron microscopy (EM). Invented in the 1930s (TEM 1931: Knoll and Ruska [24]; SEM 1937 v. Ardenne [25]), nowadays EM plainly is *the* method of fine structure investigation [26] and widely used in the field of colloid characterization [27]. However, in general the method requires ultra high vacuum (UHV) conditions in order not to scatter the fast electrons via collisions with rest gas atoms. It is obviously not possible to study aquatic colloids in their natural surrounding, and a rather time consuming sample preparation has to be performed (coating of sample with a conductive layer). Recent developments called environmental scanning electron microscopes (ESEM) allow operation at rest gas pressures of  $\sim 1$  torr. The residual gas at the same time acts as an efficient charge carrier, allowing the investigation of *uncoated* samples [28]. There are also improved preparation techniques, conserving the structure as the sample is dehydrated [29]. In all cases the sample is heated by interaction with the high-energy electrons, causing structural changes (annealing) or evaporation of atoms.

The manifold of different types of electron microscopes [30] can be subdivided into two categories: transmission electron microscopes (TEM) and scanning electron microscopy (SEM), which creates a point to point image. Secondary products (secondary electrons, backscattered electrons and X-ray photons) serve as a measure of interaction strength. These emission products (X-rays from inner shell excitation or inelastically scattered electrons) are detected from above, allow-

ing thick substrates. A very large depth of field is achieved, giving a three-dimensional impression of the objects. Particle counting and sizing is routinely performed by deposition of colloids onto a grid (or membrane after filtration) and evaluating the pictures [31]. It is a logical consequence to detect the X-rays energy-resolved by energy-dispersive spectrometry (EDS) and gain information on the elemental composition of the sample from the characteristic spectral patterns (K, L, M lines). The intensities are proportional to the respective mass concentration within the interaction volume, allowing quantitative determination of element abundance. Typical resolutions of  $\Delta E \approx 150$  eV suffice even to analyze complex colloid samples containing a multitude of elements like in natural ground-waters [31] or river and spring waters [32]. Automated micrograph evaluation algorithms allow mapping of several hundred colloids on a single particle basis as performed, e.g. for analysis of waste depository leachates [33] or natural colloids in sea sediments containing plutonium [34]. Scanning electron micrographs of suspension C are shown in Fig. 3. The suspension was dried on a substrate, rinsed with MQ-water in order to

get rid of dissolved species (salt!) and coated with a thin chromium layer. Imaging at 25 keV reveals single colloids of 15–50 nm (top, B). Due to poor resolution, smaller structures are not resolved and it is not clear whether the observed colloids are representative of the complete sample. The large particles seen in the left part of Fig. 3 could either be due to agglomeration on the substrate or represent a very small fraction of large colloids that are not detectable with PCS. However, the large agglomerates can be probed by EDS, whereas this is not possible for single small colloids due to the limited resolution in EDS mode (several 100 nm) of the microscope used here (CamScan FE44). The large agglomerate at the bottom of Fig. 3(A) results in the EDS-spectra displayed on a log scale in the lower part of Fig. 3. The Th M-lines at 2.99 keV, 3.15 keV and the L-lines at 11.1, 15.6 and 16.20 keV are clearly visible. The background is due to the Al and Si of the mica substrate and the Cr of the coating. Summarizing, SEM is a convenient standard method to get an impression on colloid size and structure for particles larger than 5 nm. Vacuum requirements and sample drying call for some preparation and no in-situ measurements are possible. The method is both destructive and invasive, and a concentrated suspension has to be provided. There are no restrictions to substrate thickness, allowing the direct analysis of particles deposited on a filter or membrane.

### 3.3. Atomic force microscopy

A completely different approach for surface investigations was introduced in 1981 by Binnig and Rohrer [35]. Imaging by use of electromagnetic radiation or particle beams was replaced by the direct interaction of an ultra-thin tip with the sample. The very first microscopes made use of the quantum mechanical tunneling effect, which allows electrons to ‘tunnel’ through a gap of several Å between two conductors. A voltage difference between tip and sample results in a current, which decreases exponentially with increasing barrier width, and serves as sensitive measure of separation. Moving the tip relative to the probe by use of piezoelectric actuators, the surface topography is

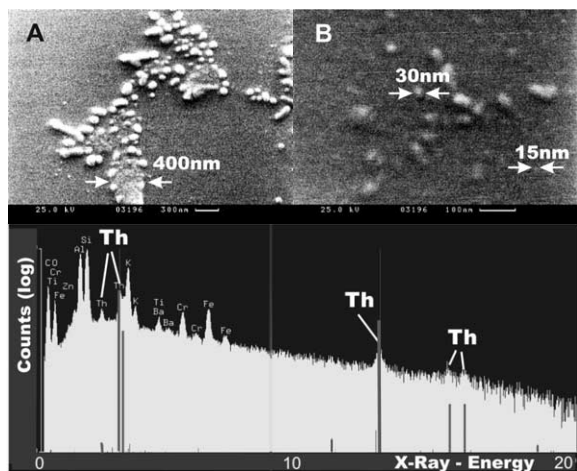


Fig. 3. The upper section shows two SEM micrographs of sample C. At regions of low coverage, single small colloids are resolved (B), whereas the particles form agglomerates at high coverage (A). The latter agglomerate results in the EDS spectra displayed at the bottom. The characteristic thorium X-ray-lines are clearly visible. Al, Si, Fe and Ti lines originate from the substrate (natural mica). Cr was used as conductive layer.

scanned. Like electron microscopy, AFM requires deposition of colloids on an atomically flat surface (e.g. mica or HOPG).

As an advantage, it can be operated in air or even in aqueous surrounding at room temperature, proving it especially suited for colloid investigations [36–40]. Although vibration isolation is recommended, resolution in the nm regime can be obtained without even a damped table. In contrast to the seemingly spatial impression SEM images offer, AFM data contain a three dimensional mapping of the surface. The vertical information is very reliable and atomic resolution is achieved, whereas lateral resolution is limited by the finite size and shape of the tip (tip artifact). Depending on the object-height and radius of the tip, the artefact may reach 50 nm, apparently increasing the diameter of a particle. The measured data has to be de-convoluted in order to obtain lateral particle dimensions as published in the case of bentonite colloids in [41]. A detailed discussion of AFM applied to investigation of colloids is given in, e.g. [27].

Samples *A* (Fig. 4) and *B* (Fig. 5) were investigated by AFM. In both images a cut along the solid line shows the vertical profile. It is

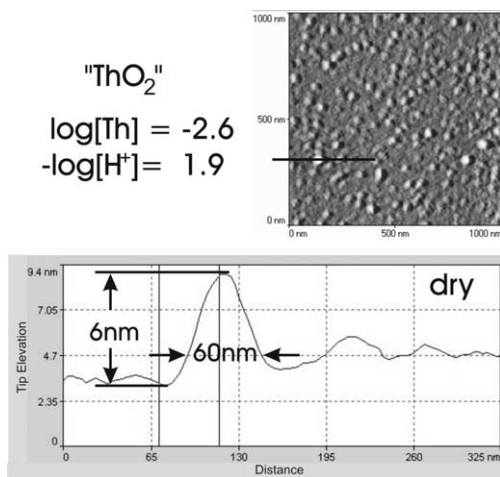


Fig. 4. AFM image of sample *A* (which was dried before measurement) and vertical profile along the solid line through one typical colloid. Averaging results in  $\approx 4\text{--}5$  nm, which agrees well with LIBD measurements, however, the lateral dimension after subtraction of the tip artefact indicates agglomeration on the substrate (details see text).

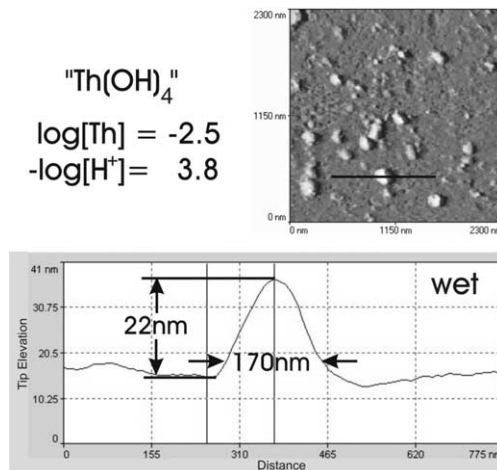


Fig. 5. AFM image of sample *B* (in wet state) and vertical profile along the solid line. As in Fig. 4, the lateral dimension does not match the height of the colloids.

obvious, that in both cases the width is much larger than the height of the particles, even after subtraction of the tip artefact. On the other hand, the vertical dimension (average 4–5 nm) is in line with the mean diameter obtained by laser induced breakdown detection (LIBD) for sample *A* (see below). For sample *B* the LIBD measurements showed a diameter of 100 nm, considerably larger than the average height in the AFM investigation (20–50 nm), but still smaller than the lateral dimension. Most likely, agglomeration occurs and small flat islands form on the charged mica substrate. The dimension of the tip (radius 50 nm) does not allow one to resolve a possible substructure.

### 3.4. Laser induced breakdown detection

In the late 1980s the lack of sensitive detection methods for small colloids in ultra-low concentrations (semiconductor manufacturing) lead to the development of LIBD [1,42]. When a pulsed laser is focused tightly into a medium (Fig. 6) exceeding a certain threshold irradiance, a so called breakdown occurs [43]: At least one atom is ionized by multi-photon ionization (MPI) early during the laser pulse, and the resulting seed electron is accelerated due to inverse bremsstrahlung in the high electric field of the laser focus. After gaining

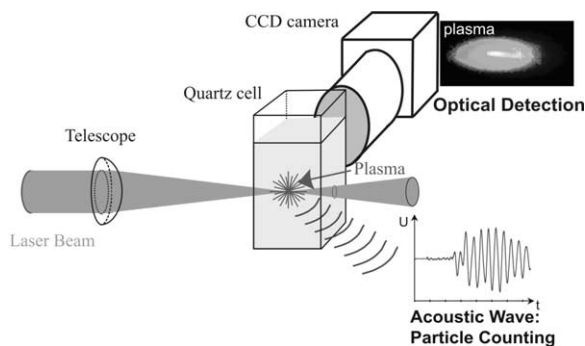


Fig. 6. LIBD, principle of operation: A plasma is ignited selectively on colloids in a suspension by a tightly focused pulsed laser. Its expansion causes an acoustic wave, which is detected by a piezo. In addition, the emitted light is observed spatially resolved by a CCD camera.

sufficient energy, additional atoms are ionized by collisions, multiplying the number of electrons. The density of free charge carriers increases in an avalanche after a few consecutive iterations and a plasma is created. However, the energy density to initiate the above process (threshold) depends on the phase of the matter in the focal region. It is highest for the gas phase, lower for liquids and lowest for bulk matter. This is made use of for particle detection: the pulse energy is adjusted such that no breakdown occurs in pure water [44]. Whenever a colloid enters the focal region, the threshold for the solid phase applies (which is exceeded) and a plasma is ignited, which can be detected by its optical emission [19,45] or by a piezo detector coupled to the sample cell, recording the acoustic signal of the plasma expansion [46,47]. By counting the number of breakdown events relative to a predefined number of laser shots (breakdown probability), the particle number density in the solution can be evaluated [48,49]. Size information is gained by determination of the breakdown probability at different energy densities: the ionization rate of a particle scales proportionally to the MPI-cross-section times the photon-flux density. The cross-section increases proportionally to the particle volume (proportional to the number of valence electrons in the particle), and hence the breakdown threshold decreases with increasing particle size and is used as a calibration curve for particle sizing. For an

unknown sample the threshold is determined by recording the breakdown probability for increasing laser pulse energies (so called s-curves, Fig. 7) and converted to a mean particle diameter [50].

Within the focal region the intensity distribution decreases from the center outwards on length scales of 2 mm along the laser beam axis and 4–5  $\mu\text{m}$  perpendicular to it (beam waist). This by far exceeds the size of the detected colloids and to good approximation the photon flux density a particle experiences is constant over its volume and does only depend on the position within the focus. By sorting the breakdown events according to their exact position within the focus, a flux dependency measurement and hence size determination is performed at a single fixed pulse energy [45]. Colloids down to  $\approx 10$  nm are detectable at concentrations as low as  $10^4$   $\text{ml}^{-1}$ , with only a linear particle size dependence as shown in Fig. 2. Bimodal [50] or narrow [2] particle size distributions (20–100 nm) are accessible directly. Systems containing a large fraction of colloids  $> 1000$  nm have to be pre-fractionated, for instance by filtration or FFF [51].

It is important to note that the method requires some kind of calibration with monodisperse particles of well defined size (usually polystyrene

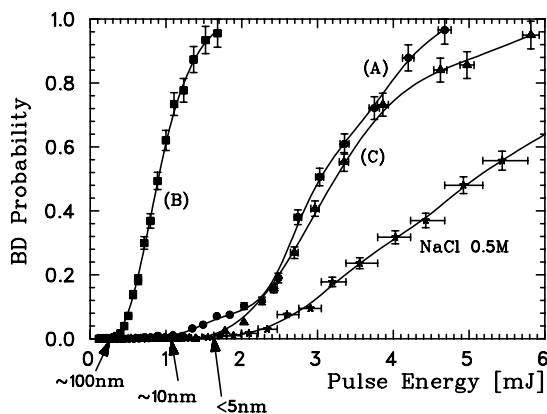


Fig. 7. All three samples are measured by LIBD without preparation or pre-fractionation and the breakdown (BD) probability as function of laser pulse energy, so-called s curves, are plotted. The energy threshold allows to determine the weighted mean particle size (arrows below x-axis). While B and C show a narrow size distribution, the saddle of A at low BD probability indicates a higher polydispersity.

reference colloids). Strictly speaking, this calibration of threshold versus particle-size is only valid for this very material. For different materials the calibration might be wrong by up to a factor of 2 [49]. In consequence, the calibration has either to be repeated for the new material (if reference colloids are available), or the thresholds have to be converted using a model [48,50], which requires the ionisation potential and the MPI cross-section of the colloids. The former is easily found in standard literature [52] and can be corrected for small size and surface effects [53], but the latter generally is not known and must be calculated [54,55] by the Keldysh theory [56] or determined experimentally [57].

Summarizing, LIBD is a sensitive (ppt), method to detect single nanoparticles down to 5 nm diameter directly in liquid, without need for preparation. The method is non-invasive but destructive in the sense that the very particle measured is vaporized in the plasma. However, typically only a small fraction ( $10^5$  particles) of the total particle content is decomposed, and the suspension as a whole is only marginally affected allowing consecutive observations of long term colloid alteration [58,59]. Reliable, even mobile systems were built and successfully applied to in-situ field studies of colloid migrations [60,61].

Applied to the  $\text{ThO}_n(\text{OH})_m$ -colloids, LIBD confirms the large colloid size for *B*. The sample *A* ( $\text{ThO}_2$  colloids) shows a breakdown threshold corresponding to  $\sim 10$  nm with a rather large saddle below 10% BD-probability, indicating some polydispersivity of the system. This is probably due to formation of small (2–5 nm) primary colloids which agglomerate over time. Suspension *C* exhibits a similar curve in the upper part, but with almost no saddle, hence suggesting a narrow size distribution of (2–5 nm). Due to the inherent high sensitivity of the method, LIBD measurements are also sensitive to colloidal contamination stemming from primary chemicals. It is indispensable to perform ‘background measurements’ of all chemicals used in the experiments. In our case this is the matrix, a 0.5 M NaCl solution. After twofold recrystallization and ultrafiltration the matrix is of sufficient purity and does not contribute considerably to the total colloid content (Fig. 7, ‘NaCl’).

Recently, a new LIBD apparatus was developed, applying an excimer-pumped dye-laser (Lambda Scanmate). The excitation wavelength can be tuned continuously, while the pulse energy is kept constant by a home built attenuator-feedback-loop. As described above, LIBD is based on multi-photon ionization, which, in general is a non-resonant process. Tuning the wavelength of the laser allows the use of material dependent resonances in analogy to the well known resonance enhanced multi-photon ionization process (REMPI) [62–64] used to investigate atoms and molecules in the gas phase. This ‘REMPI-LIBD’ was applied to samples *A* and *B* as shown in Fig. 8. While sample *B*, exhibits two pronounced absorption patterns at 480 and 450 nm, no significant enhancement is seen for the ‘ $\text{ThO}_2$ ’ species (*A*). This result is surprising, because in both cases the thorium ion is bound in its tetravalent state. The difference is the coordination by two oxygen atoms in case *A* in contrast to four OH-groups in case *B*. Hence, REMPI-LIBD is not only sensitive to the valence state, but even to the first coordination shell of the thorium ion. A quantitative interpretation would involve spectroscopic information (absorption spectra, level schemes) on  $\text{ThO}_2$  and  $\text{Th}(\text{OH})_4$ . While the former is available in literature, to our knowledge no data exists on amorphous precipitates of the latter.

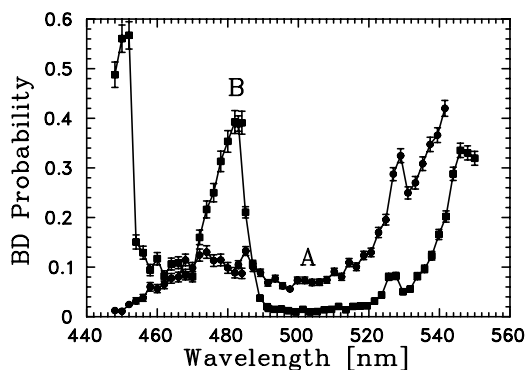


Fig. 8. Breakdown (BD) probability as function of excitation wavelength measured by an excimer pumped dye-laser system. The samples were neither prepared nor prefractionated. Sample *B* exhibits two pronounced absorption patterns at 480 and 450 nm, but no significant enhancement is seen for the ‘ $\text{ThO}_2$ ’ species (*A*).

Hence, for the time being, this finding will only be of phenomenological nature.

A direct proof of the different composition of colloids *A* and *B* was found by transmission electron microscopy (TEM): In contrast to SEM, TEM makes use of electrons transmitted through the sample and calls for thin samples (of the order of 10–100 nm) in order not to absorb the electron beam and reduce multiple scattering of electrons. For the same reason the sample has to be water free. Suspensions *A* and *B* were dried on a TEM grid (carbon film on gold mesh) and imaged in a 300 keV transmission microscope. Due to the NaCl content of the suspension most colloids were embedded in NaCl crystals. Only a few single colloids were found, and hence the pictures might not be representative of the whole sample. The right part of Fig. 9 shows a  $\text{Th}(\text{OH})_4$ -colloid of suspension *B* at 270 000-fold magnification. Its diameter of some 50 nm is still in line with the LIBD measurements, considering the low statistics of the TEM images. However, this particle exhibits substructure and seems to consist of small (3–5 nm) colloids. This confirms the assumption that the large particles of strongly over-saturated  $\text{Th}(\text{OH})_4$  suspensions are agglomerates of small primary colloids.

The left part of Fig. 9 shows a colloid of the ‘ $\text{ThO}_2$ ’ domain. In contrast to the LIBD measurements, where the majority of particles was detected in the  $>10$  nm regime, no such particles were observed. Only larger colloids (10–50 nm) from

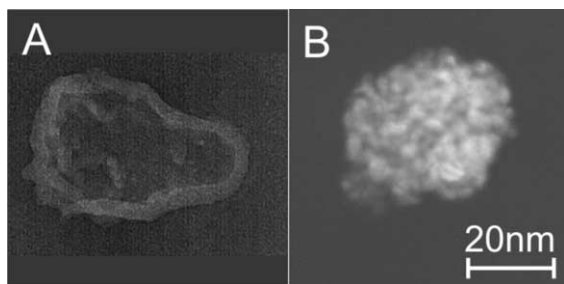


Fig. 9. TEM micrographs of samples *A* and *B*. Sample (*A*) shows a core-layer structure of presumably microcrystalline  $\text{Th}(\text{O})_2$  (see Fig. 10) surrounded by an amorphous phase containing additional water or hydroxo-species. The amorphous colloid of sample *B* is composed of small spherical ‘sub-particles’, the structure of which is not known.

the ‘saddle’ of the breakdown curve were found. This could be due to low contrast. Even the 50 nm particle of Fig. 9(left) is hard to see against the substrate. Nevertheless the image allows the distinction of a core and a brighter outer layer of a few nanometer thickness. Both particles were further examined by transmission electron diffraction (TED). The spatial resolution of  $\approx 100$  nm allowed us to image diffraction patterns of the single colloids of Fig. 9. Particle *A* revealed a clear pattern (Fig. 10). The dark regions (high electron flux) correspond to strong diffraction of the (111) plane with a spacing of 3.1 Å. This is in qualitative agreement with the  $\text{ThO}_2$  bulk value of 3.23 Å, but disagrees with findings of Dzimitrowicz et al., that the precipitate of Th(IV) has fluorite structure with a spacing of 3.4 Å [65]. While the latter group initiated rapid precipitation, great care was taken in our experiments to approach the solubility curve very slowly, so formation of colloids might proceed differently than in a precipitation experiment and lead to a more highly ordered structure. However, the diffraction patterns prove unambiguously the existence of a crystalline phase inside the colloid. For particle *B* no diffraction was observed. In consequence the particle either is completely amorphous, or it is composed of many small crystallites which are randomly oriented and

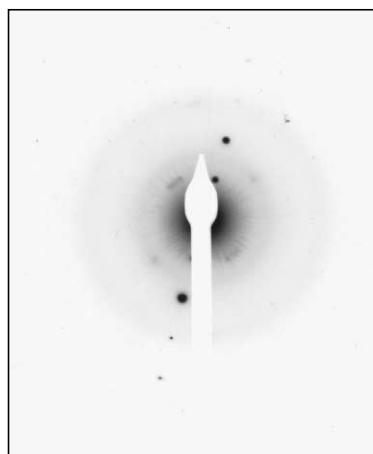


Fig. 10. Electron diffraction pattern of the single colloid shown in Fig. 9(A). The pattern indicates a lattice spacing of 3.1 Å in agreement with bulk crystalline  $\text{ThO}_2$  (3.23 Å). The direct beam is shadowed in order to avoid saturation.

don't show a net diffraction, as is plausible from the substructure visible in Fig. 9.

#### 4. Concluding remarks

Table 2 summarizes all data obtained for the three samples *A*, *B*, and *C*. The results for sample *A*, the crystalline colloids, are in satisfactory agreement: LIBD and SEM suggest 10 nm or below, while AFM yields an average value of 4–5 nm, and consistently PCS cannot detect any colloids since at this small size light scattering needs higher concentrations. In the TEM investigations we find a distribution of larger colloids. This is due to the low contrast of small particles and sample preparation. The suspension contains 0.5 M NaCl, and we cannot rinse the TEM grid after deposition without washing off the colloids as well. Hence, most colloids were embedded in NaCl crystallites, which was verified by electron-diffraction, and only very few clean thorium particles were found, leading to poor statistics. TED proved the crystallite structure of the particles with a (111) plane spacing of 3.1 Å in the core and an amorphous layer.

Sample *B* contains larger colloids due to the higher degree of oversaturation [66] (SEM: 50–100 nm, TEM 50 nm, LIBD  $\approx$  100 nm) of amorphous structure (TED), which are composed of smaller substructures (TEM), which in turn might have crystalline structure [65,21]. The AFM data of the

vertical dimension, as for sample *A*, suggest smaller colloids. This might be due to a size selectivity of the adhesive forces and the attachment process to the mica, favoring smaller particles. The data of the lateral dimension shows a larger spread (up to several 100 nm), which cannot be explained by the tip artefact (50 nm). The reason most likely is the formation of agglomerates on the substrate, observed commonly during the drying process of substrates and attributed to capillary forces [67]. Had there been particles much larger than 100 nm preformed in the suspension, PCS should have given a clear signal, because the colloid-concentration of  $\approx$  1 ppm is just below the limit of detection for 100 nm and PCS is much more sensitive for larger colloids. In addition the breakdown threshold of LIBD would have been shifted to lower pulse energies considerably, even if only  $<$  1% of all particles had been larger than 100 nm [50]. REMPI measurements show two resonance patterns at 450 and 480 nm which are not observed for sample *A* and indicate a difference in coordination. So far the peaks could not be assigned to known molecular resonances.

The least information could be obtained for sample *C* due to the low thorium colloid concentration. Neither by TEM nor by AFM (wet state) were any colloids found on the substrate. The particles observed by SEM were agglomerates, which formed during the dehydration process and allowed us to perform EDS. LIBD suggests 2–5 nm size, which explains the lack of signal by PCS. REMPI investigations were not performed.

The above data are shown merely to demonstrate the capability of the respective methods. A detailed discussion on theoretical grounds will follow along with further long term investigations on colloid stability [66]. However, it should be evident that even the investigation of a relatively simple laboratory sample (only two colloidal species—ThO<sub>2</sub> and Th(OH)<sub>4</sub>) requires a multitude of different methods. For natural samples which cover a much larger size range and in general have a complex chemical composition, this holds true all the more, emphasizing that colloid science is a highly interdisciplinary field.

Table 2  
Summary of the results for Samples *A*, *B* and *C* described in detail in the respective sections

	<i>A</i>	<i>B</i>	<i>C</i>
[Th]	$2.5 \times 10^{-3}$ M	$3 \times 10^{-3}$ M	$6.3 \times 10^{-5}$ M
pH	1.9	3.8	4.1
PCS	No signal	No signal	No signal
SEM	$<$ 10 nm	$<$ 50–200 nm	15–50 nm + agglomerates
EDS	No signal	No signal	Th lines (Fig. 3)
AFM	4–5 nm	20–50 nm	No signal
LIBD	$\approx$ 10 nm	100 nm	2–5 nm
REMPI	No pattern	2 resonances	Not investigated
TEM	10–50 nm	$\approx$ 50 nm	No signal
TED	X-tal 3.1 Å	Amorphous	No signal

## Acknowledgements

I am indebted to many people who contributed to the work shown here. In alphabetical order I thank C. Bitea (LIBD), J.I. Kim (former head of the institute), V. Neck (Th-solubility), M. Plaschke (AFM), J. Römer and K. Spieler (SEM), T. Schäfer (PCS), P. Schlossmacher (TEM) and I. Yun (LIBD). In addition, I am grateful to H. Geckeis and F.J. Scherbaum for many valuable discussions and proof reading.

## References

- [1] T. Kitamori, K. Yokose, K. Suzuki, T. Sawada, Y. Goshi, *Jpn. J. Appl. Phys.* 27 (6) (1988) L983.
- [2] M. Bolz, W. Hoffmann, W. Rühle, F. Becker, *Wat. Chem. Nucl. React. Sys.* 7 (1996) 42.
- [3] C. Degueldre, A. Bilewicz, H.P. Alder, *Nucl. Sci. Eng.* 120 (1995) 65.
- [4] C. Degueldre, E. Schenker, H. Nobbenhuis-Wedda, *Wat. Chem. Nucl. React. Sys.* 7 (1996) 112.
- [5] H.P. Alder, C. Degueldre, E. Schenker, *Wat. Chem. Nucl. React. Sys.* 7 (1996) 272.
- [6] C.B. Murray, D.J. Norris, M.G. Bawendi, *J. Am. Chem. Soc.* 115 (1993) 8706.
- [7] K. Riwotzki, H. Meyssamy, H. Schnablegger, A. Kornowsky, M. Haase, *Angew. Chem.* 113 (3) (2001) 574.
- [8] W. Moser, *Advanced Catalysts and Nanostructured Materials*, Academic Press, San Diego, 1996.
- [9] T. Baumann, N. Huber, S. Müller, R. Nießner, *Vom Wasser* 95 (2000) 151.
- [10] J.I. Kim, *Mater. Res. Soc. Bull.* 19 (12) (1994) 47.
- [11] A.B. Kersting, D.W. Efurud, D.L. Finnegan, D.J. Rokop, D.K. Smith, J.L. Thompson, *Nature* 397 (1999) 56.
- [12] J.I. Kim, B. Kanellakopoulos, *Radiochim. Acta* 48 (1989) 145.
- [13] R. Knopp, V. Neck, J.I. Kim, *Radiochim. Acta* 86 (1999) 101.
- [14] J.I. Kim, P. Zeh, B. Delakwitz, *Radiochim. Acta* 58 (1992) 147.
- [15] H.G. Barth, B.E. Boyes, C. Jackson, *Anal. Chem.* 70 (1998) 215.
- [16] T.F. Rees, *Wat. Resour. Res.* 26 (11) (1990) 2777.
- [17] H. Cölfen, M. Antonietti, *Adv. Polym. Sci.* 150 (2000) 67.
- [18] C. Degueldre, H.-R. Pfeiffer, W. Alexander, B. Wernli, R. Bruetsch, *Appl. Geochem.* 11 (5) (1996) 677.
- [19] T. Bundschuh, R. Knopp, R. Müller, J.I. Kim, V. Neck, T. Fanghänel, *Radiochim. Acta* 88 (2000) 625.
- [20] J. Rothe, M.A. Denecke, V. Neck, R. Müller, J.I. Kim, *Inorg. Chem.* 41 (2002) 249.
- [21] V. Neck, R. Müller, M. Bouby, M. Altmaier, J. Rothe, M.A. Denecke, J.I. Kim, *Radiochim. Acta*, 21 (2002) 485–494.
- [22] A. Ledin, S. Karlsson, A. Düker, B. Allard, *Wat. Res.* 28 (7) (1994) 1539.
- [23] L. Rayleigh, *Philos. Mag.* 41 (1871) 107.
- [24] M. Knoll, E. Ruska, *Ann. Phys.* 12 (1932) 607.
- [25] M. v. Ardenne, *Z. Phys.* 109 (1938) 553.
- [26] S.L. Flegler, J.W. Heckman, K.L. Klomparens, *Scanning and Transmission Electron Microscopy*, Oxford University Press, Oxford, 1993.
- [27] G.L. Hornyaka, S. Peschela, T. Sawitowska, G. Schmid, *Micron* 29 (2–3) (1998) 183.
- [28] H.E. Nuttal, R. Kale, *Micr. Res. Techn.* 25 (1993) 439.
- [29] E. Balnois, K.J. Wilkinson, *Coll. Surf. A*, 207 (2002) 229–242.
- [30] P. Rennert, H. Schmiedel, C. Weißmantel, *Kleine Enzyklopädie Physik, i Editio*, Harri DeutschThun, Frankfurt, 1987.
- [31] C. Degueldre, I. Triay, J.I. Kim, P. Vilks, M. Laaksoharju, N. Miekeley, *Appl. Geochem.* 15 (2000) 1043.
- [32] O. Atteia, D. Perret, T. Adatte, R. Kozel, P. Rossi, *Environ. Geol.* 34 (4) (1998) 257.
- [33] T. Klein, R. Niessner, *Vom Wasser* 87 (1996) 373.
- [34] M. Moring, T.K. Ikäheimonen, R. Pöllänen, E. Ilus, S. Klemola, J. Juhanaja, M. Eriksson, *J. Radioanal. Nucl. Chem.* 248 (3) (2001) 623.
- [35] G. Binnig, H. Rohrer, C. Gerber, E. Weibel, *Appl. Phys. Lett.* 40 (1982) 178.
- [36] C. Degueldre, *Mater. Res. Symp. Proc.* 465 (1997) 835.
- [37] K.J. Wilkinson, E. Balnois, G.G. Leppard, *J. Buffle, Colloid Surf. A* 28 (1999) 155.
- [38] P.H. Santschi, E. Balnois, K.J. Wilkinson, J. Zhang, J. Buffle, L. Guo, *Limnol. Oceanogr.* 43 (1998) 896.
- [39] M. Plaschke, J. Römer, R. Klenze, J.I. Kim, *Colloid Surf. A* 160 (1999) 269.
- [40] M. Plaschke, J. Römer, R. Klenze, J.I. Kim, *Surf. Interface Anal.* 30 (2000) 297.
- [41] M. Plaschke, T. Schäfer, T. Bundschuh, N.M. Thang, R. Knopp, H. Geckeis, J.I. Kim, *Anal. Chem.* 73 (2001) 4338.
- [42] T. Kitamori, K. Yokose, M. Sakagami, T. Sawada, *Jpn. J. Appl. Phys.* 28 (7) (1989) 1195.
- [43] L.J. Radziemski, D.A. Cremers, *Laser induced Plasmas and Applications*, Marcel Dekker, Rochester, 1989.
- [44] C.A. Sacchi, *J. Opt. Soc. Am. B* 8 (2) (1991) 337.
- [45] T. Bundschuh, W. Hauser, J.I. Kim, R. Knopp, F.J. Scherbaum, *Colloid Surf. A* 180 (2001) 285.
- [46] W. Hauser, *FZK-Bericht* 9057 (1998) 1.
- [47] W. Hauser, R. Götz, *Patent (Germany)* DE 19602048C2.
- [48] F.J. Scherbaum, R. Knopp, J.I. Kim, *Appl. Phys. B* 63 (1996) 299.
- [49] T. Bundschuh, R. Knopp, J.I. Kim, *Colloid Surf. A* 177 (2001) 47.
- [50] C. Walther, C. Bitea, W. Hauser, J.I. Kim, F.J. Scherbaum, *Nucl. Instr. Methods B*, 195 (2002) 374–388.
- [51] N.G. Thang, R. Knopp, H. Geckeis, J.I. Kim, H.P. Beck, *Anal. Chem.* 72 (1) (2000) 1.

- [52] D.R. Lide, *Handbook of Chemistry and Physics*, 75th Edition, CRC Press, Boston, 1995.
- [53] H. Burtscher, U. Mueller, A. Schmidt-Ott, *Z. Phys. D* 12 (1–4) (1989) 563.
- [54] J. Schwarz, P. Rambo, J.C. Diels, *Appl. Phys. B* 72 (3) (2001) 343.
- [55] C.J.G.J. Uiterwaal, C.R. Gebhardt, H. Schröder, K.-L. Kompa, *Phys. Rev. Lett.*, in press.
- [56] L.V. Keldysh, *Sov. Phys. JETP* 20 (5) (1965) 1307.
- [57] C. Walther, A. Herlert, J.I. Kim, F.J. Scherbaum, L. Schweikhard, M. Vogel, *Chem. Phys.* 265 (2001) 243.
- [58] V. Neck, J.I. Kim, B.S. Seidel, C.M. Marquardt, K. Dardenne, M.P. Jensen, W. Hauser, *Radiochim. Acta* 89 (2001) 1.
- [59] C. Bitea, C. Walther, J.I. Kim, H. Geckeis, T. Rabung, F.J. Scherbaum, D. Cacuci, *Colloid Surf. A*, in press.
- [60] W. Hauser, H. Geckeis, J.I. Kim, T. Fierz, *Colloid Surf. A* 203 (1–3) (2002) 37.
- [61] W. Hauser, R. Götz, H. Geckeis, B. Kienzler, Äspö progress report.
- [62] U. Boesl, J. Grottemeyer, K. Walter, E.W. Schlag, Resonance ionisation and time-of-flight mass spectrometry: high resolution, involatile molecules, In: RIS 86, Vol. 84, *Inst. Phys. Conf. Ser.*, pp. 223.
- [63] J.C. Miller, C.S. Feigerle, Multiphoton ionization of transient species in supersonic jets, In: RIS 88, Vol. 94, *Inst. Phys. Conf. Ser.*, pp. 101.
- [64] T. Gibert-Legrand, T. Gonthiez, L. Vivet, P. Brault, Resonant ionisation mass spectrometry of ammonia, In: RIS 98, The American Institute of Physics, pp. 143.
- [65] D.J. Dzimitrowicz, P.J. Wiseman, D. Cherns, *J. Colloid Interface Sci.* 103 (1) (1985) 170.
- [66] C. Bitea, R. Müller, V. Neck, C. Walther, J.I. Kim, *Colloid Surf. A*, this issue.
- [67] A. Thill, O. Spalla, *Colloid Surf. A*, this issue.